Case Studies in Thermal Engineering 27 (2021) 101326

Contents lists available at ScienceDirect

Case Studies in Thermal Engineering

journal homepage: www.elsevier.com/locate/csite

Determining the critical insulation thickness of breathing wall: Analytical model, key parameters, and design

Chong Zhang [a,b,*], Jinbo Wang [a,**]

[a] Department of Building Environment and Energy Engineering, Huazhong University of Science and Technology, Wuhan, China
[b] Department of Building Services Engineering, The Hong Kong Polytechnic University, Kowloon, Hong Kong, China

ARTICLE INFO

Keywords:
Thermal insulation
Air preheating
Critical thickness
Darcy's law
Breathing wall
Building ventilation

ABSTRACT

Breathing wall (BW) based on air-permeable porous medium offers an alternative solution for utilizing the conductive heat loss of building envelope to preheat the infiltration ventilation airflow within porous medium. However, current studies neglect the influence of pressure drop within porous medium on the energy performance of BW, which may lead to an overestimation or non-optimal design. In this study, we proposed a framework to determine the critical insulation thickness of BW for minimizing its convective heat loss and pressure drop related energy loss. An analytical model was developed and validated to calculate the heat loss of BW under third-type boundary condition. Darcy's law was applied to estimate the pressure drop of infiltration airflow and its associated energy loss. Case studies were conducted to identify the critical insulation thickness of BW. The critical thickness of BW under different scenarios was investigated. The results demonstrate the existence of critical thickness, which yields the lowest overall heat loss of BW. A larger infiltration airflow rate or lower air permeability of porous medium will result in a downward trend of this critical thickness. The outcomes of this study can provide a design guideline of BW for maximizing its energy saving potential.

1. Introduction

Ventilation is necessary for all kind of buildings to provide sufficient outdoor air, which can help to maintain an acceptable indoor air quality (IAQ) and suitable thermal environment [1]. It is estimated that in most commercial and industrial buildings, ventilation accounts for around 30% and 25% of heat loss, respectively [2]. Therefore, a variety of technologies have been developed and utilized to decrease the heat loss due to the ventilation, such as: heat recovery device, earth-to-air heat exchanger, and etc. The heat recovery device is commonly used in mechanical ventilation system to achieve energy exchange between indoor exhaust air and outdoor fresh air [3]. The earth to air heat exchanger assisted ventilation system can utilize the shallow geothermal to preheat the cold ventilation air in winter [4]. Therefore, seeking some approaches that can satisfy the needs of building ventilation as well as energy-saving is significant for buildings.

Currently, some innovation technologies are developed to integrate the ventilation into building envelope for reducing the heat loss due to the ventilation in heating-dominated climates, for instance, supply air window (or called as ventilated window) and breathing

* Corresponding author. Department of Building Environment and Energy Engineering, Huazhong University of Science and Technology, Wuhan, China.
** Corresponding author.
E-mail addresses: chong0324.zhang@polyu.edu.hk (C. Zhang), jbwang@hust.edu.cn (J. Wang).

https://doi.org/10.1016/j.csite.2021.101326
Received 22 April 2021; Received in revised form 13 July 2021; Accepted 8 August 2021
Available online 10 August 2021

Nomenclature

BW	breathing wall
c	specific heat, J/(kgK)
E	power, W
EER	energy efficiency ratio
G	airflow volume, m^3/s
h	heat transfer coefficient, W/m^2K
k	permeability, m^2
L	thickness, m
Nu	Nusselt number
Pe	Péclet number
Q	heat loss, W
T	temperature, K
u	infiltration airflow rate, m/s
WWR	window to wall ratio
η	efficiency
ρ	density, kg/m^3
λ	thermal conductivity, W/mK
μ	dynamic viscosity of air, Pa s
ΔP	pressure drop, Pa

Subscripts

a	air
ce	convection at exterior surface
ci	convection at interior surface
e	electromotor
fan	fan
in	interior surface or indoor
loss	overall heat loss
m	modified
n	normalized
out	outdoor
p	porous medium
pe	exterior surface of porous medium
pi	interior surface of porous medium
re	radiation at exterior surface
ri	radiation at interior surface

wall. For the supply air window [5], the cold ventilation air driven by natural buoyancy force flows through the air-gap between the glazing panes and is preheated by conductive heat loss and absorbed solar heat therein, and eventually enters the indoor space. Further improvement of preheating capacity can be achieved by designing a U-shape triple-glazing supply air window, since the heat exchange area between the ventilation air and glazing is extended [6]. Such a kind of window design provides a combination of building ventilation and air preheating, which can help to reduce the domestic heating energy demand and improve the IAQ [7].

Breathing wall (BW), or called as dynamic insulation, offers an alternative solution for utilizing the conductive heat loss of opaque building envelope to preheat the ventilation air in heating-dominated climates, which can effectively reduce the heating energy demand of building ventilation [8]. The schematic and mechanism of the BW are illustrated in Fig. 1. The porous and air-permeable material is the crucial component of the BW [9]. Driven by the stack effect or additional mechanical fan, the ambient air adjacent to BW is sucked into the indoor space through the porous medium. The interaction of ventilation airflow (from outdoor to indoor) and conductive heat flux (from indoor to outdoor) within the BW can act as a contra-flux heat exchanger in winter. Ventilation air exchanges heat with the porous medium and is preheated by the conductive heat flux before entering the buildings in winter. Similar structure can be found in porous medium based exhaust air insulation wall [10], which utilizes the exfiltration airflow within the porous medium to prevent the conductive heat gain of wall.

The concept of BW is initially applied to agricultural buildings in some European countries (e.g. Norway, Sweden, Germany, etc.) [11]. The investigations of this unconventional insulating technique gradually focus on its application in residential buildings due to its potential advantages, including but not limited to natural ventilation [12], air filtering performance [13], and energy saving [14]. In recent years, Ascione et al. [15] explored the integration of nocturnal free cooling into the BW for enhancing the indoor thermal comfort in summer. Alongi et al. designed a special apparatus called the Dual Air Vented Thermal Box, conducted a series of experimental investigation on the steady-state [8] and dynamic thermal behavior [16] of BW, and fully validated the conventional analytical

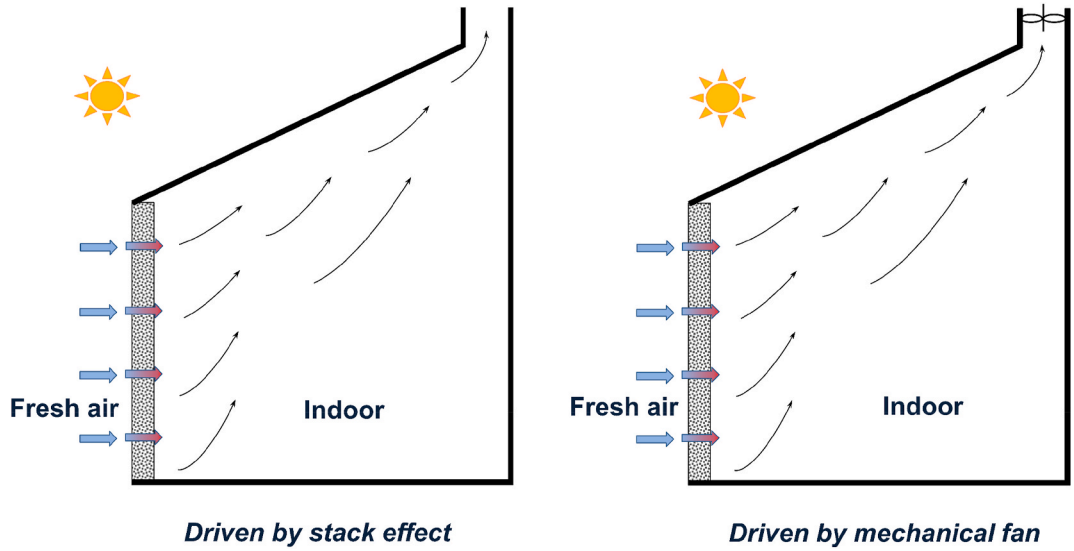

Fig. 1. Schematic of the breathing wall.

model as well as a new proposed steady periodic analytical model [17]. Craig and Grinham [9] carried out a fundamental and theoretical work to identify the influence of the flowing air on the heat exchange at the surface of porous materials and provided the correlating equations of the mixed convection at the surface of the BW. Craig et al. [18] designed and optimized mass timber panels based BW module to achieve a reduction of embodied and operational carbon emissions.

The promising ventilation and thermal performance of the BW is mainly attributed to the infiltration process within the porous and air-permeable material. The infiltration airflow of the BW is driven by a certain pressure difference that can be achieved by either natural ventilation (e.g. utilizing the stack effect or wind activity) or mechanical ventilation (e.g. by fans). However, natural ventilation is more challenging to design since the wind speed, direction, and site conditions will influence the operation of the BW to a great extent [19]. Mechanical ventilation of BW is easier to design, permits a greater choice of site, and is more predictable in operation, but it will incur additional energy consumption.

Therefore, mechanical ventilation may be essential for practical application of the BW. Previous studies indicate that the heat loss and U-value of the BW can be decreased to approximately zero with the increase of the thickness of porous medium. In the meanwhile, increasing the thickness of porous medium would increase the pressure drop of infiltration process and energy loss due to the mechanical ventilation. It means that energy consumption of mechanical ventilation will offset the energy saving of the BW to a certain extent. There must exist a critical thickness of porous medium, which can achieve the minimum overall energy loss, when

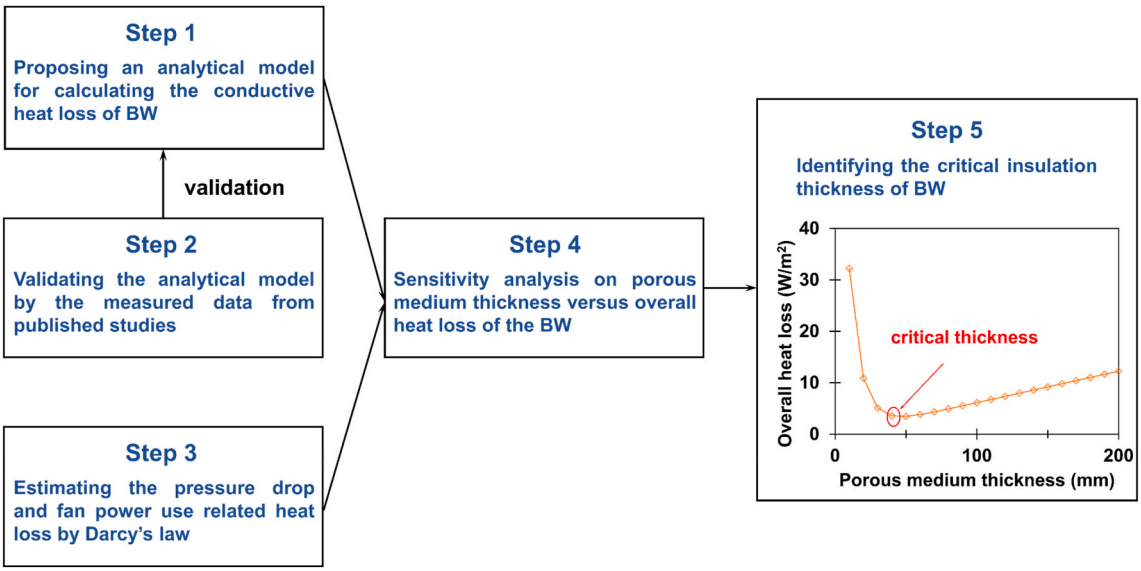

Fig. 2. Flowchart for determining the critical thickness of porous medium.

simultaneously considering the convective heat loss and energy loss due to mechanical ventilation. Therefore, such a critical thickness of porous medium should be estimated for maximizing the energy saving potential of the BW.

The main purposes of this study are to provide a method to identify the critical thickness of air-permeable porous medium for minimizing the overall energy loss of the BW, and provide its design guideline for practical application. In this study, a steady-state analytical model was proposed to calculate the surface temperature of the BW under third-type boundary condition. For the model validation, the calculated surface temperatures were compared with the measurement data obtained from published studies. Darcy's law was used to estimate the pressure drop of infiltration process within porous medium, and the energy loss due to mechanical ventilation was further calculated. Case studies was carried out to evaluate the influence of porous medium thickness on the overall energy loss of the BW and identify the critical thickness of porous medium. Moreover, the critical thickness under different scenarios was also investigated and discussed.

2. Methodology

The flowchart for determining the critical thickness of porous medium is presented in Fig. 2. In this study, investigations only focus on the heat transfer and pressure drop of porous medium component, and other possible components of the BW are not considered. Such a treatment is commonly used in previous studies of the BW.

2.1. Analytical model of breathing wall

Heat transfer and airflow within the BW can be treated as one-dimensional process. Moreover, the direction of ventilation airflow is opposite to the direction of conductive heat flux within the porous medium, as shown in Fig. 3. The infiltration ventilation airflow (from outdoor to indoor) absorbs part of the conductive heat flux (from indoor to outdoor). This makes the convective heat loss from exterior surface of BW to ambient environment (Q_{out}) is much lower than the convective heat loss from indoor space to interior surface of BW (Q_{in}). For the BW, as illustrated in Fig. 3, convective heat loss at interior surface (Q_{in}) is equal to convective heat loss at exterior surface (Q_{out}) plus thermal energy for air preheating ($Q_{preheat}$). Although the use of BW will increase the convective heat loss at interior surface of wall (Q_{in}), most of this heat loss is utilized to preheat the ventilation airflow. Therefore, the heat loss at the exterior surface of BW (Q_{out}) is commonly used to analyze the thermal performance and evaluate the U-value of the BW in previous studies.

Due to the high-porosity and light-weight character, heat storage capacity of the BW is commonly neglected, and steady-state model is adopted to analyze the thermal performance of the BW in winter [8]. In this study, one-dimensional steady-state model proposed by Taylor et al. [20] was used to analyze the conduction and advection within the BW, as expressed in Eq. (1). The horizontal ventilation airflow was assumed to be thermal equilibrium with the adjacent porous aggregates.

$$\lambda_p \frac{\partial^2 T_p}{\partial x^2} - \rho_a c_a u \frac{\partial T_p}{\partial x} = 0 \tag{1}$$

where c_a and ρ_a are specific heat capacity and density of air; λ_p is thermal conductivity of porous medium; u is infiltration airflow rate within porous medium in horizontal direction. The analytical solution of the one-dimensional steady-state model is defined as follows.

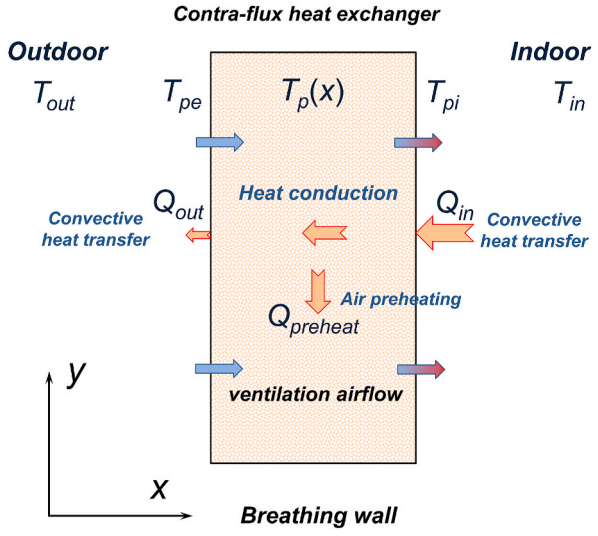

Fig. 3. Heat transfer and airflow within the BW.

$$\frac{T_p(x)-T_{pe}}{T_{pi}-T_{pe}}=\frac{\exp\left(\frac{\rho_a c_a u}{\lambda_p}x\right)-1}{\exp\left(\frac{\rho_a c_a u}{\lambda_p}L_1\right)-1} \tag{2}$$

where T_{pi} and T_{pe} are interior surface temperature and exterior surface temperature of BW, respectively; L_p is thickness of porous medium. Based on the Fourier's law of heat conduction, the one-dimensional heat conduction within the BW can be further expressed as Eq. (3).

$$q_c=-\lambda_p\frac{\partial T_p}{\partial x}=-\rho_a c_a u\frac{\exp\left(\frac{\rho_a c_a u}{\lambda_p}x\right)}{\exp\left(\frac{\rho_a c_a u}{\lambda_p}L_p\right)-1}\left(T_{pi}-T_{pe}\right) \tag{3}$$

The energy balance equations for the interior and exterior surfaces of the BW based on third-type boundary condition are established as:

$$h_e\left(T_{out}-T_{pe}\right)+\rho_a c_a u\left(T_{out}-T_{pe}\right)=-\rho_a c_a u\frac{\left(T_{pi}-T_{pe}\right)}{\exp\left(\frac{\rho_a c_a u}{\lambda_p}L_p\right)-1} \tag{4}$$

$$h_i\left(T_{pi}-T_{in}\right)=-\rho_a c_a u\frac{\exp\left(\frac{\rho_a c_a u}{\lambda_p}L_p\right)}{\exp\left(\frac{\rho_a c_a u}{\lambda_p}L_p\right)-1}\left(T_{pi}-T_{pe}\right) \tag{5}$$

where h_i and h_e are combined convective-radiative heat transfer coefficients at interior and exterior surfaces of the BW, respectively; T_{in} and T_{out} are indoor and outdoor air temperature, respectively. The model characteristic parameters are defined as:

$$x=\rho_a c_a u \tag{6}$$

$$k=\exp\left(\frac{\rho_a c_a u}{\lambda_p}L_p\right) \tag{7}$$

The deduction of the energy balance equations can obtain the analytical expressions of the temperatures of the exterior and interior surfaces of BW. The analytical expressions are given below:

$$T_{pe}=\frac{T_{out}kx^2+[T_{out}h_i(k-1)+T_{in}h_i+T_{out}h_e k]x+T_{out}h_i h_e(k-1)}{kx^2+k(h_i+h_e)x+h_e h_i(k-1)} \tag{8}$$

$$T_{pi}=\frac{T_{out}kx^2+k(T_{out}h_e+T_{in}h_i)x+T_{in}h_i h_e(k-1)}{kx^2+k(h_i+h_e)x+h_e h_i(k-1)} \tag{9}$$

The heat loss at exterior surface of the BW (Q_{out}) is defined as Eq. (10).

$$Q_{out}=h_e\left(T_{pe}-T_{out}\right) \tag{10}$$

Based on this analytical model, the heat loss of a specific design BW can be easily calculated, with given the boundary conditions (i.e. airflow rate within porous medium, indoor temperature, and outdoor sol-air temperature).

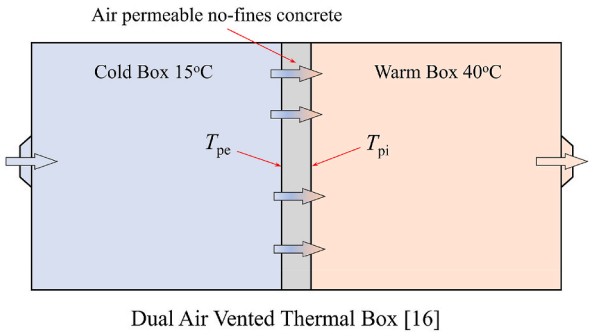

Fig. 4. Schematic of the steady state experimental analysis of the BW.

2.2. Model validation

In our previous studies, an experimental rig has been established to experimentally test the thermal performance of a porous medium based air-permeable wall under different boundary conditions [10]. However, the temperature at one of the porous medium's surfaces has not been recorded. In this study, therefore, the measurement results reported by Alongi et al. [16] were used to validate the analytical expressions of the exterior and interior surface temperatures of BW.

A well-designed Dual Air Vented Thermal Box was built by Alongi et al. [16] to perform a series of experimental investigation of the BW. The schematic of this apparatus is illustrated in Fig. 4. Two thermal boxes with the internal dimension of 1.29 m × 1.22 m × 1.22 m (length × width × height) are used to simulate the indoor and outdoor environment, respectively. A test sample of BW is installed in-between the two thermal boxes. The porous medium is the no-fines concrete with a thickness of 15 cm, and its thermal conductivity is 1.24 W/(m·K). The temperatures of two thermal boxes are maintained at 15 °C and 40 °C for the steady-state experimental analysis, respectively. Five different ventilation airflow rates are considered. More detailed information about the experimental test of the BW under steady-state boundary conditions can refer to the Ref. [16].

The combined convective-radiative heat transfer coefficients at the exterior and interior surfaces of the BW were calculated according to the theoretical investigations proposed by Craig and Grinham [9]. The studies carried out a schlieren imaging experiment to demonstrate that the ventilation airflow will significantly influence the convection boundary layers at the two surfaces of the BW. The sucked airflow at exterior surface of BW will lead to a thinner boundary layer and reduce the thermal resistance, and in the meanwhile, the blowing airflow at interior surface of BW will lead to a thicker boundary layer and enhance the thermal resistance. The correlation equations provided in Ref. [9] were used to calculate the convective heat transfer coefficients for the model validation. To determine the radiative heat transfer coefficients, assuming the radiant temperature was equal to the air temperature of the thermal box in this study. The calculated convective and radiative heat transfer coefficients at the central nodes of exterior and interior surfaces of the BW under different airflow rates are listed in Table 1. Pe is Péclet number; Nu_n and Nu_m are normalized and modified [9] Nusselt number; h is heat transfer coefficient, and definition of each subscript is presented in Nomenclature. It can be found that the calculated convective heat transfer coefficients reproduce the phenomenon of variable boundary layer of BW observed by Craig and Grinham [9].

To validate the analytical model, the airflow rate, air temperature of cold box, and air temperature of warm box were the inputs of the analytical expressions, and then the calculated exterior surface temperature and interior surface temperature of the BW were compared with corresponding measured results reported in Ref. [16], as shown in Fig. 5 and Table 2. It can be found that the calculated and measured surfaces temperatures show good agreement. The maximum deviation of 1 °C occurs at the calculated exterior surface temperature (T_{pe}) with an airflow rate of 0.001 m/s. Apart from that the deviations of the calculated results are basically within ±0.4 °C. The average absolute deviations of the calculated T_{pe} and T_{pi} are 0.39 °C and 0.29 °C, respectively. Therefore, it can be concluded that the analytical expressions proposed in this study can calculate the surface temperatures of the BW with good accuracy.

2.3. Pressure drop of infiltration process within porous medium

The pressure drop of the ventilation airflow within the BW was calculated based on Darcy's law, as shown in Eq. (11). The law reveals the correlation between the pressure drop (ΔP), airflow rate within porous medium (u), dynamic viscosity of air (μ), and thickness (L_p) and permeability (k_p) of porous medium. The air permeability (k_p/μ) of the commonly used porous medium can be obtained from the Ref. [21].

$$\Delta P = \frac{\mu L_p u}{k_p} \tag{11}$$

The fan power (E_{fan}) due to the mechanical ventilation of the BW can be further calculated as Eq. (12).

$$E_{fan} = \frac{G\Delta P}{\eta_e \eta_{fan}} \tag{12}$$

where G is the airflow volume per unit area of the BW, m^3/s; η_{fan} and η_e are the fan efficiency and electromotor efficiency, and the overall efficiency ($\eta_e \times \eta_{fan}$) of 0.55 [22] is adopted for the mechanical fan. The energy efficiency ratio (EER) for space heating is assumed to 4.5 for a typical air source heat pump system. Moreover, to estimate the overall heat loss of the BW, the fan power (E_{fan}) transfers into its corresponding heat loss (Q_{fan}). The heat loss due to the mechanical ventilation is expressed as: $Q_{fan} = E_{fan} \times EER$.

Table 1
Calculated convective and radiative heat transfer coefficients.

Airflow rate (m/s)	Exterior surface adjacent to cold side				Interior surface adjacent to warm side			
	$\sqrt{Pe}/Nu_n$	Nu_m/Nu_n	h_{ce}	h_{re}	$\sqrt{Pe}/Nu_n$	Nu_m/Nu_n	h_{ci}	h_{ri}
0.001	0.12	1.06	2.06	5.61	0.11	0.98	2.01	6.68
0.003	0.22	1.22	2.21	5.57	0.18	0.95	2.04	6.62
0.006	0.35	1.58	2.49	5.51	0.24	0.87	1.99	6.53
0.009	0.50	2.15	2.94	5.47	0.29	0.77	1.80	6.48
0.012	0.68	3.04	3.51	5.45	0.32	0.65	1.56	6.42

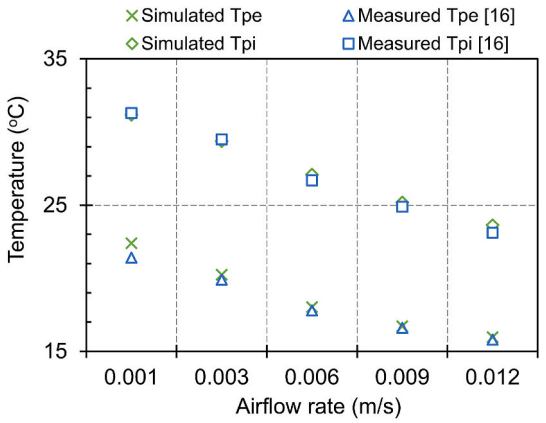

Fig. 5. Comparison of simulated surface temperatures and measured data.

Table 2
Comparison of the calculated and measured [16] surface temperatures.

Airflow rate (m/s)	Exterior surface temperature (°C)		Interior surface temperature (°C)	
	Measured	Calculated	Measured	Calculated
0.001	21.4	22.4	31.3	31.2
0.003	19.9	20.2	29.5	29.4
0.006	17.8	18.0	26.7	27.1
0.009	16.6	16.7	24.9	25.2
0.012	15.8	16.0	23.1	23.6

Finally, the overall heat loss of the BW in winter can be calculated as:

$$Q_{loss} = Q_{out} + Q_{fan} \tag{13}$$

3. Case studies for determining the critical insulation thickness

In this study, the influence of porous medium thickness on the overall heat loss of the BW was evaluated to determine its critical thickness for achieving the minimum overall heat loss. Due to the high-porosity and light-weight character of the BW, the steady boundary conditions in typical winter design day were adopted in this study for determining the critical thickness of the BW. Moreover, it should be noticed that the proposed framework for determining the critical insulation thickness of the BW can be easily extended to various weather conditions or cities and different types of buildings (e.g. residential building, office building, school building, and etc.)

3.1. Simulation conditions

In this study, a typical office room with the size of 6 m × 4 m × 3 m (length × width × height) was adopted for case studies. The BW was employed as the only external wall with the size of 4 m × 3 m (width × height). The ventilation airflow rate of the room was set to 61.9 m^3/h based on ANSI/ASHRAE Standard 62.1–2019 [1]. Three different window-to-wall ratios (WWRs) including 30 %, 40 %, and 50 % were considered. For the WWRs of 30 %, 40 %, and 50 %, the frontal areas of the BW were 8.4 m^2, 7.2 m^2, and 6 m^2, which correspond the infiltration airflow rates of 0.0021 m/s, 0.0024 m/s and 0.0029 m/s, respectively.

Heating design conditions of Beijing (cold climate zone) were adopted in the case studies. Outdoor dry bulb temperature and indoor temperature are −10.9 °C and 20 °C, respectively. The combined convective-radiative heat transfer coefficients at the exterior and interior surfaces of the BW were considered as the constant and equal to 23.26 W/m^2K and 8.3 W/m^2K, respectively. Moreover, three types of commonly used air-permeable porous media were also considered. The thermophysical properties of the used porous media are listed in Table 3.

Table 3
Material properties. Note: 1 derived from Ref. [13]; 2 derived from Ref. [21].

Material	Thermal conductivity (W/mK)	Air permeability (m^2/sPa)
Mineral fiber insulation[1]	0.045	1.83E-05
Light-weight concrete[2]	0.367	2.22E-04
Cellulose insulation[2]	0.038	1.22E-06

3.2. Effect of key parameters

Fig. 6 shows the effect of porous medium thickness on the overall heat loss of the BW with different WWRs. The overall heat loss of the BW consists of the convective heat loss and heat loss due to fan power consumption. Mineral fiber insulation was employed as the porous medium of the BW. The thickness ranges from 10 mm to 200 mm with an interval of 10 mm. The results in Fig. 6(a) indicate that increasing the porous medium thickness can effectively reduce the convective heat loss at the exterior surface of BW. As the porous medium thickness increases to 70 mm, the convective heat loss will decrease to 0.71 W/m^2, 0.41 W/m^2, and 0.16 W/m^2 for the BW with the WWR of 30 %, 40 %, and 50 %, respectively. Such a promising performance is mainly because a thicker porous medium will enlarge heat exchange area and contact time between the porous medium and infiltration airflow, and then improve the air-preheating efficiency of the BW. Previous studies [14] pointed out similar results that the proper design of porous medium thickness and airflow rate can decrease the U-value as well as the convective heat loss of the BW to near-zero. Moreover, larger WWR means higher infiltration airflow rate within the porous medium, which results in a reduction of the convective heat loss. When the WWR varies from 30

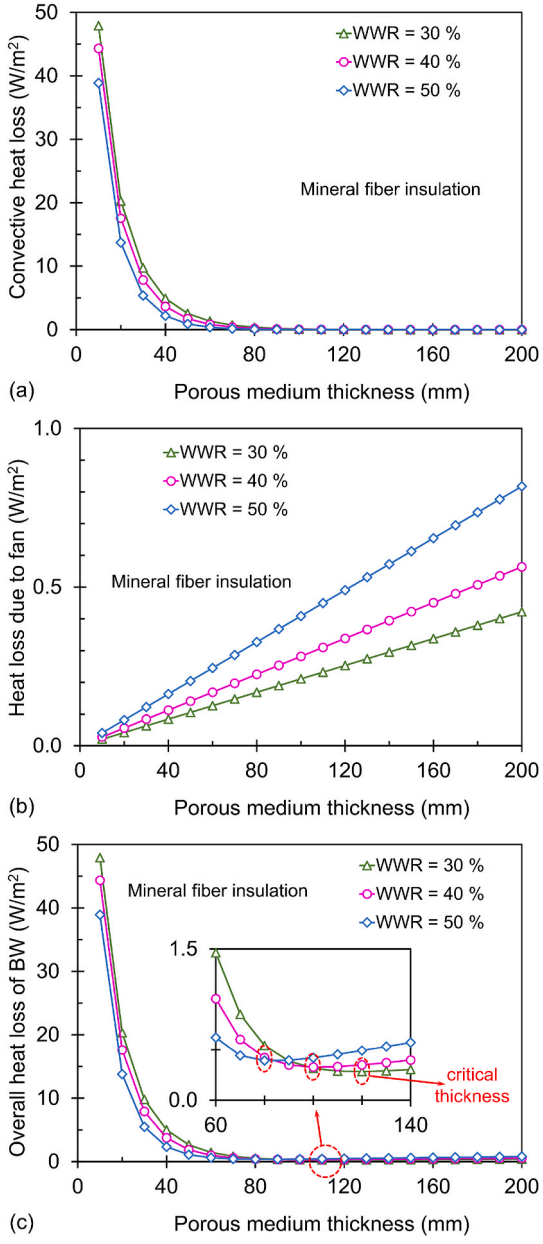

Fig. 6. Effect of porous medium thickness on the: (a) convective heat loss, (b) heat loss due to fan power, and (c) overall heat loss, of the BW with different WWRs.

% to 50 %, the convective heat loss will decrease from 47.9 W/m^2 to 38.9 W/m^2 for the BW with a porous medium thickness of 10 mm.

As shown in Fig. 6(b), the porous medium thickness versus the heat loss due to fan power consumption exhibits a linear variation. It can be found that the heat loss due to fan power consumption gradually enlarge with the increase of porous medium thickness. Moreover, the scenario of 50 % WWR shows a highest heat loss compared with other two WWRs. When the WWR varies from 30 % to 50%, the heat loss due to fan power consumption increases from 0.42 W/m^2 to 0.82 W/m^2. Such a result can be explained by Darcy's law in Eq. (11).

The results in Fig. 6(c) demonstrate the existence of critical thickness, which yields the lowest overall heat loss of the BW. This critical insulation thickness can achieve a compromise between the convective heat loss and fan power consumption related heat loss. It means that when the porous medium thickness exceeds to this critical value, the increment of fan power related heat loss will offset the reduction of convective heat loss. Therefore, further increment of the porous medium thickness may be meaningless. Moreover, the critical insulation thickness are 120 mm, 100 mm, and 80 mm for the BW with the WWR of 30 %, 40 %, and 50 %, respectively. A downward trend of this critical thickness can be observed with the increase of WWR.

To further identify the influence of the thermophysical properties of porous medium on the critical insulation thickness of the BW,

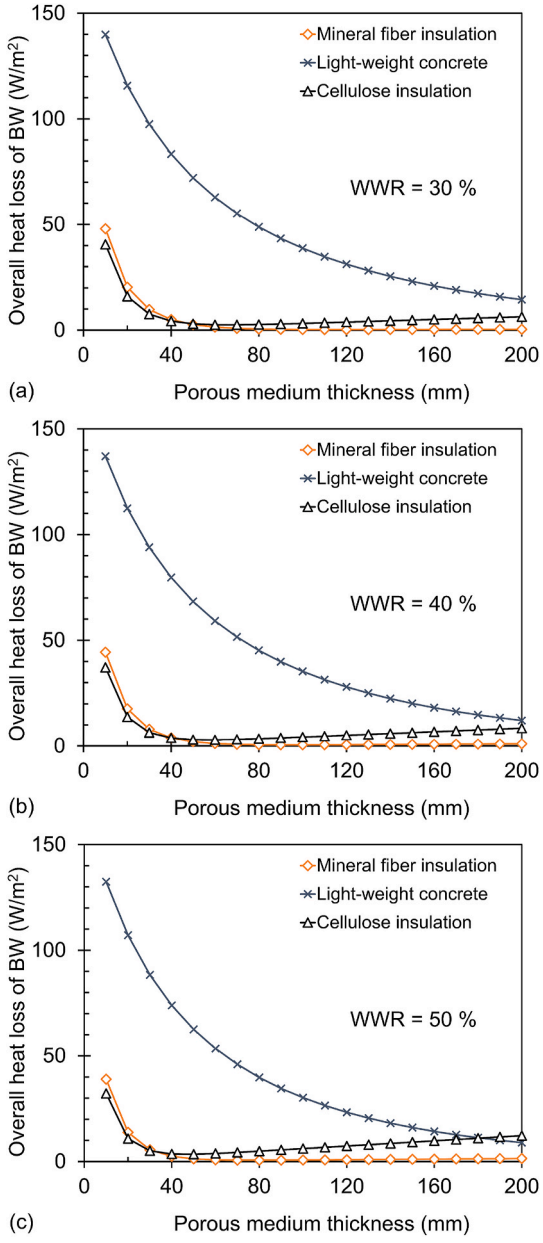

Fig. 7. Effect of porous medium thickness on the overall heat loss of BW with the: (a) WWR of 30 %, (b) WWR of 40 %, (c) WWR of 50 %.

three commonly used porous media in the research field of BW were investigated and compared. As shown in Table 3, cellulose insulation has the lowest thermal conductivity and air permeability, and on the contrary, light-weight concrete has the highest thermal conductivity and air permeability. This means that cellulose insulation shows a better thermal insulation property than mineral fiber insulation and light-weight concrete for preventing the conductive heat loss. However, cellulose insulation will lead to the highest fan power consumption for driving the infiltration ventilation airflow.

Fig. 7 presents the variation of porous medium thickness versus overall heat loss for the BW with different porous media. The results indicate that the selection of porous medium exhibits a significant influence on the overall heat loss of the BW. Light-weight concrete has the highest overall heat loss because of its poor thermal insulation property. Moreover, due to the high air permeability of light-weight concrete, it makes the fan power consumption related heat loss of light-weight concrete is almost one-tenth of the value of mineral fiber insulation and one-hundredth of the value of cellulose insulation, respectively. And consequently, the pressure drop and corresponding fan power consumption of the light-weight concrete can be neglected within the normal range of the thickness of building envelope wall. This can well explain why no critical insulation thickness can be observed for light-weight concrete in Fig. 7.

As shown in Fig. 7, the variation curve of the porous medium thickness versus overall heat loss for the cellulose insulation shows an obvious corner. Owing to the lowest air permeability, the use of cellulose insulation will lead to a higher pressure drop and corresponding fan power consumption. This will increase the proportion of fan power related heat loss in the overall heat loss of BW, and consequently result in a downward trend of the critical thickness. Compared to the critical thickness of mineral fiber insulation, the use of cellulose insulation decreases the critical thickness from 120 mm, 100 mm, and 80 mm–70 mm, 60 mm, and 50 mm for the BW with the WWR of 30 %, 40 %, and 50 %, respectively. Moreover, for the scenario of BW with a WWR of 50 %, the overall heat loss of the cellulose insulation increases from 3.5 W/m^2 to 12.3 W/m^2 when the thickness various from the critical value to 200 mm. It means that for the porous medium with a relatively low air permeability, the fan power consumption related heat loss is a non-negligible portion of the overall heat loss, and its critical thickness should be estimated for minimizing the overall heat loss of the BW.

4. Conclusions

In this study, we proposed a framework to determine the critical insulation thickness of the BW for achieving its minimum overall heat loss. An analytical model was developed to calculate the convective heat loss of the BW with third-type boundary condition. The proposed model has been validated by comparing the calculated results with measured data obtained from published studies. Moreover, Darcy's law was adopted to estimate the pressure drop of the ventilation airflow within the porous medium, and its corresponding fan power consumption can be calculated. Case studies were carried out to evaluate the influence of porous medium thickness on the overall heat loss of the BW in a typical office room, and to further identify the critical thickness of porous medium. The critical insulation thickness of the BW under different scenarios was also investigated. The main outcomes of this studies can be concluded as follows: (1) This study demonstrates the existence of critical insulation thickness which can yield the lowest overall heat loss of the BW, when considering the pressure drop of ventilation infiltration airflow; (2) When the porous medium thickness reached to or exceeds the critical value, further increasing the porous medium thickness is meaningless or will enlarge the overall heat loss of the BW; (3) The critical thickness of the mineral fiber insulation are 120 mm, 100 mm, and 80 mm for the BW with the WWR of 30 %, 40 %, and 50 %, respectively. These critical values will decrease to 70 mm, 60 mm, and 50 mm for the application of cellulose insulation. Increasing the WWR or employing a porous medium with relatively low air permeability will result in a downward trend of the critical thickness; (4) For most situations, the pressure drop can not be neglected, and the critical insulation thickness of the BW should be estimated for maximizing its energy-saving potential. Moreover, it should be noticed that the proposed framework for determining the critical insulation thickness of the BW can be extended to various weather conditions and building types (e.g. residential building, office building, school building, and etc.)

CRediT authorship contribution statement

Chong Zhang: Methodology, Investigation, Formal analysis, Visualization, Funding acquisition, Writing – original draft, Writing – review & editing. **Jinbo Wang:** Conceptualization, Supervision, Writing – review & editing.

Declaration of competing interest

The authors declare that they have no known competing financial interests or personal relationships that could have appeared to influence the work reported in this paper.

Acknowledgement

The studies are supported by the grant (No. 51808239) of National Natural Science Foundation of China, and grant (No. XJ2019044) of Hong Kong Scholars Program.

References

[1] ASHRAE. ANSI/ASHRAE, Standard 62.1-2019, Ventilation for Acceptable Indoor Air Quality, American Society of Heating, Refrigerating and Air-Conditioning Engineers, Inc, Atlanta, GA, 2019.

[2] CIBSE Charted Institution of Building Services Engineers, CIBSE Top Tips-Ventilation in Buildings, 2015. https://www.cibse.org/knowledge/knowledge-items/detail?id=a0q20000006oamlAAA.
[3] P.M. Cuce, S. Riffat, A comprehensive review of heat recovery systems for building applications, Renew. Sustain. Energy Rev. 47 (2015) 665–682.
[4] H. Li, L. Ni, G. Liu, Y. Yao, Performance evaluation of Earth to Air Heat Exchange (EAHE) used for indoor ventilation during winter in severe cold regions, Appl. Therm. Eng. 160 (2019) 114111.
[5] M. Bhamjee, A. Nurick, D.M. Madyira, An experimentally validated mathematical and CFD model of a supply air window: forced and natural flow, Energy Build. 57 (2013) 289–301.
[6] F. Gloriant, A. Joulin, P. Tittelein, S. Lassue, Using heat flux sensors for a contribution to experimental analysis of heat transfers on a triple-glazed supply-air window, Energy 215 (2021) 119154.
[7] F. Gloriant, P. Tittelein, A. Joulin, S. Lassue, Study of the performances of a supply-air window for air renewal pre-heating, Energy Procedia 78 (2015) 525–530.
[8] A. Alongi, A. Angelotti, L. Mazzarella, Experimental investigation of the steady state behaviour of Breathing Walls by means of a novel laboratory apparatus, Build. Environ. 123 (2017) 415–426.
[9] S. Craig, J. Grinham, Breathing walls: the design of porous materials for heat exchange and decentralized ventilation, Energy Build. 149 (2017) 246–259.
[10] C. Zhang, J. Wang, L. Li, W. Gang, Dynamic thermal performance and parametric analysis of a heat recovery building envelope based on air-permeable porous materials, Energy 189 (2019) 116361.
[11] T. Græe, Breathing Building Construction, ASEA Stillwater, Oklahoma, 1974.
[12] D.W. Etheridge, J.J. Zhang, Dynamic insulation and natural ventilation: feasibility study, Build. Serv. Eng. Technol. 19 (1998) 203–212.
[13] B.J. Taylor, R. Webster, M. S Imbabi, The building envelope as an air fiter, Build. Environ. 34 (1999) 353–361.
[14] B.J. Taylor, M.S. Imbabi, The application of dynamic insulation in buildings, Renew. Energy 15 (1998) 377–382.
[15] F. Ascione, N. Bianco, C.D. Stasio, G.M. Mauro, G.P. Vanoli, Dynamic insulation of the building envelope: numerical modeling under transient conditions and coupling with nocturnal free cooling, Appl. Therm. Eng. 84 (2015) 1–14.
[16] A. Alongi, A. Angelotti, L. Mazzarella, Measuring a Breathing Wall's effectiveness and dynamic behaviour, Indoor Built Environ. 29 (2020) 783–792.
[17] A. Alongi, A. Angelotti, L. Mazzarella, Experimental validation of a steady periodic analytical model for Breathing Walls, Build. Environ. 168 (2020) 106509.
[18] S. Craig, A. Halepaska, K. Ferguson, P. Rains, J. Elbrecht, A. Freear A, et al., The design of mass timber panels as heat-exchangers (dynamic insulation), Front. Built. Environ. 6 (2021) 606258.
[19] B.J. Taylor, M.S. Imbabi, Environmental design using dynamic insulation, Build. Eng. 106 (2000) 15–28.
[20] B.J. Taylor, D.A. Cawthorne, M.S. Imbabi, Analytical investigation of the steady-state behaviour of dynamic and diffusive building envelopes, Build. Environ. 31 (1996) 519–525.
[21] M.K. Kumaran, IEA-annex 24 on Heat, Air and Moisture Transfer in Insulated Envelope Parts: Task 3 Material Properties, Final Report, 1996. Leuven.
[22] Y. El Fouih, P. Stabat, P. Rivière, P. Hoang, V. Archambault, Adequacy of air-to-air heat recovery ventilation system applied in low energy buildings, Energy Build. 54 (2012) 29–39.